are likely to have evolved in response to these substantial changes in ejaculate characteristics. As an example, *A. gambiae* females synthesize significantly lower levels of 20E after blood feeding compared with *A. albimanus* (*7*, *21*), indicating a possible adaptation of female 20E to levels transferred by the male. The observed effects of the male 20E-MISO interaction in regulating egg development suggest that the evolution of sexually transferred 20E will have influenced other blood-feeding–induced processes, with possible consequences for parasite transmission. Notably, a role for ecdysone in mediating protozoan parasite development has been reported in a number of insect species [reviewed in (*22*)], including other vectors of human disease (*23*).

Our phylogenetic approaches combined with phenotypic analyses of multiple reproductive traits provide considerable insight into a group of important disease vectors. Multiple key entomological parameters that directly affect malaria transmission are influenced by the diverse functions of sexually transferred 20E: mosquito densities via MISO-mediated increased oogenesis (*5*); parasite development through the expression of lipid transporters that protect *Plasmodium* from the mosquito immune system (*8*); and longevity due to reduced mating-associated fitness costs (*9*–*11*). Consequently, divergent sexual transfer of 20E across anophelines may have shaped their ability to transmit this deadly disease, and, intriguingly, all four species that transfer large levels of 20E are major malaria vectors originating from Africa and India, the regions of highest malaria burden (*1*). By demonstrating correlated evolution in male ejaculate characters and parallel changes in female physiology implicated in vectorial capacity, we reveal coevolutionary dynamics likely to have fundamentally influenced disease transmission to humans.

REFERENCES AND NOTES

1. World Health Organization, *World Malaria Report 2014* (WHO, Geneva, 2014).
2. G. MacDonald, *Bull. World Health Organ.* **15**, 613–626 (1956).
3. B. Yuval, *Annu. Rev. Entomol.* **51**, 413–440 (2006).
4. E. Pondeville, A. Maria, J. C. Jacques, C. Bourgouin, C. Dauphin-Villemant, *Proc. Natl. Acad. Sci. U.S.A.* **105**, 19631–19636 (2008).
5. F. Baldini *et al.*, *PLOS Biol.* **11**, e1001695 (2013).
6. P. Gabrieli *et al.*, *Proc. Natl. Acad. Sci. U.S.A.* **111**, 16353–16358 (2014).
7. H. Bai, D. B. Gelman, S. R. Palli, *Pest Manag. Sci.* **66**, 936–943 (2010).
8. M. K. Rono, M. M. Whitten, M. Oulad-Abdelghani, E. A. Levashina, E. Marois, *PLOS Biol.* **8**, e1000434 (2010).
9. T. Chapman, L. F. Liddle, J. M. Kalb, M. F. Wolfner, L. Partridge, *Nature* **373**, 241–244 (1995).
10. S. Wigby, T. Chapman, *Curr. Biol.* **15**, 316–321 (2005).
11. A. Dao *et al.*, *J. Med. Entomol.* **47**, 769–777 (2010).
12. M. Bownes, A. Dubendorfer, T. Smith, *J. Insect Physiol.* **30**, 823–830 (1984).
13. J. C. Perry, L. Sirot, S. Wigby, *Trends Ecol. Evol.* **28**, 414–422 (2013).
14. S. M. Lewis, A. South, *Adv. Stud. Behav.* **44**, 53–97 (2012).
15. M. K. Lawniczak *et al.*, *Trends Ecol. Evol.* **22**, 48–55 (2007).
16. D. E. Neafsey *et al.*, *Science* **347**, 1258522 (2015).
17. S. H. Alonzo, T. Pizzari, *Am. Nat.* **175**, 174–185 (2010).
18. S. H. Alonzo, T. Pizzari, *Philos. Trans. R. Soc. Lond. B Biol. Sci.* **368**, 20120044 (2013).
19. S. A. West, A. S. Griffin, A. Gardner, *Curr. Biol.* **17**, R661–R672 (2007).
20. B. Walsh, *Genetica* **118**, 279–294 (2003).
21. Y. H. Lu, H. H. Hagedorn, *Int. J. Inver. Reprod. Develop.* **9**, 79–94 (1986).
22. P. O. Lawrence, *In Vitro Cell. Dev. Biol.* **27**, 487–496 (1991).
23. M. R. Cortez *et al.*, *Exp. Parasitol.* **131**, 363–371 (2012).

ACKNOWLEDGMENTS

We thank E. Lund and D. Clarke for help with mosquito rearing and insectary procedures and M. Bernardi for assistance with artwork. We are grateful to D. Neafsey and N. Besansky for numerous helpful discussions and to S. Lewis, D. Neafsey, M. Mota, and members of the Catteruccia laboratory for careful reading of the manuscript. This work was sponsored in part by the following grants awarded to F.C.: a European Research Council FP7 ERC Starting Grant (grant Anorep, ID: 260897), a William F. Milton Fund grant (Harvard Medical School 2013), and an NIH grant (grant ID: NIH 1R01AI104956-01A1). S.N.M., E.G.K., A.S., and F.C. designed the experiments. P.I.H. provided experimental material, and S.N.M., E.G.K, and P.I.H. performed the experiments. S.N.M., E.G.K, A.S., and R.M.W. analyzed the data. S.N.M., E.G.K., A.S., and F.C. wrote the manuscript. S.N.M., E.G.K., and A.S. contributed equally to this study. All gene sequences are freely available via given gene identifiers from VectorBase (www.vectorbase.org). The single-copy ortholog sequences used to produce the species phylogeny are available via OrthoDB (http://cegg.unige.ch/orthodbmoz2). Protein sequence alignments employed for the species and MISO-AGAP002621 phylogenies are available via DRYAD: doi:10.5061/dryad.6f576.

SUPPLEMENTARY MATERIALS

www.sciencemag.org/content/347/6225/985/suppl/DC1
Materials and Methods
Figs. S1 and S2
References (*24*–*32*)

31 July 2014; accepted 16 January 2015
10.1126/science.1259435

CLIMATE CHANGE

Atlantic and Pacific multidecadal oscillations and Northern Hemisphere temperatures

Byron A. Steinman,[1]* Michael E. Mann,[2] Sonya K. Miller[2]

The recent slowdown in global warming has brought into question the reliability of climate model projections of future temperature change and has led to a vigorous debate over whether this slowdown is the result of naturally occurring, internal variability or forcing external to Earth's climate system. To address these issues, we applied a semi-empirical approach that combines climate observations and model simulations to estimate Atlantic- and Pacific-based internal multidecadal variability (termed "AMO" and "PMO," respectively). Using this method, the AMO and PMO are found to explain a large proportion of internal variability in Northern Hemisphere mean temperatures. Competition between a modest positive peak in the AMO and a substantially negative-trending PMO are seen to produce a slowdown or "false pause" in warming of the past decade.

Distinguishing between forced and unforced variability in climate is critical for assessing the impact of anthropogenic forcing on temperature, drought, hurricane activity, weather extremes, and other climate phenomena. The North Atlantic and North Pacific oceans are the key drivers of internal variability in Northern Hemisphere temperatures on multidecadal time scales, but there is substantial uncertainty in their relative contributions to the observed variability. We applied a new semi-empirical method that uses a combination of observational data and a large ensemble of coupled climate model simulations to assess the relative roles of both forced and internal variability in the Northern Hemisphere over the historical period.

The Atlantic Multidecadal Oscillation (AMO) (*1*) is the leading mode of internal variability in North Atlantic sea surface temperature (SST) on multidecadal (~50 to 70 years) time scales (*2*–*4*). The Pacific Decadal Oscillation (PDO) (*5*, *6*) is the leading mode of North Pacific internal SST variability but, as defined, consists of at least two distinct signals, one roughly bidecadal with a ~16- to 20-year period and the other multidecadal with a ~50- to 70-year period (*4*, *7*–*9*). The PDO and AMO time series typically are defined in terms of the temporal pattern of temperature change in the north-central Pacific and North Atlantic, respectively. The multidecadal component of the PDO may in part be related to the AMO [although centered in the Atlantic, it appears (*2*, *3*) to project at least weakly onto the Pacific] and in part reflective of low-frequency variability related to the El Niño–Southern Oscillation (ENSO) and its extratropical response (*10*–*16*). We distinguish the multidecadal component from the conventionally defined PDO by terming it the "PMO," and we term the multidecadal component of internal Northern Hemisphere mean temperature variability the "NMO."

Prior methods used to define these internal variability components and their influence on Northern Hemisphere temperature include (i) a simple linear detrending of the mean North Atlantic SST time series (*17*–*21*), (ii) estimating the forced trend based on regression of North Atlantic SST against global mean SST and

---

[1] Large Lakes Observatory and Department of Earth and Environmental Sciences, University of Minnesota Duluth, Duluth, MN, USA. [2] Department of Meteorology and Earth and Environmental Systems Institute, Pennsylvania State University, University Park, PA, USA.
*Corresponding author. E-mail: bsteinma@d.umn.edu

Downloaded from www.sciencemag.org on February 26, 2015

removing the forced trend to yield an estimate of the internal variability (*16*, *22*, *23*), and (iii) defining the forced component as the mean of North Atlantic SST in an ensemble of climate model simulations and defining the internal variability component as the difference between the observed SST series and the multimodel mean (*24*, *25*). These methods, as shown below, do not in general yield correct results. We estimated the Atlantic and Pacific-basin multidecadal internal variability components and their contribution to Northern Hemisphere temperature change on the basis of a new target region regression approach.

Our method is based on the principle that internal variability is uncorrelated among distinct realizations of a large ensemble. We therefore used the mean of the Coupled Model Intercomparison Project Phase 5 (CMIP5) ensemble (*26*) as an initial estimate of the forced component of surface temperature for the North Atlantic, North Pacific, and the entire (land + ocean) Northern Hemisphere region (Fig. 1). The estimated forced series is rescaled via linear regression against the actual temperature series so as to accommodate potential differences in the amplitude of the true forced response relative to the multimodel mean response (for example, because of disparities in climate sensitivity). We define the AMO, PMO, and NMO as the difference between the observations and estimated, regional forced temperature series for each of the three respective regions, low-pass filtered at a frequency of 40 years in order to isolate multidecadal variability (*27*).

We analyzed both the subensemble of simulations (n = 24) of the GISS-E2-R model (*28*) (henceforth "CMIP5-GISS"); the subensemble of simulations (n = 45) of models (M = 15) with aerosol indirect effects ("CMIP5-AIE"); and the larger, full (n = 170 total realizations) ensemble of all (M = 44) models ("CMIP5-All") (Fig. 1, fig. S1, and table S1). The three ensembles are complementary in their characteristics. The GISS-E2-R simulations (which comprise the largest CMIP5 ensemble for an individual model) are consistent in their forcings and include representation of the first aerosol indirect effect (cloud albedo). The CMIP5-AIE models all have full representations of both the first and second (cloud lifetime) indirect aerosol effects, which are potentially important contributions to the net radiative forcing (*29*). The CMIP5-All ensemble provides a much larger sample, but individual simulations vary in the forcings that were used and how they were implemented. Recent work (*30*) has explored the hypothesis that at least some of the difference between modeled and observed temperature changes arises from errors in the forcing estimates (for example, the accumulated effects of small volcanic eruptions over the past decade are not accounted for in the vast majority of CMIP5 simulations). Our assumption is that these three different ensembles mean estimates of the forced temperature signal span a representative range of uncertainty in the underlying forcing.

In defining the AMO, PMO, and NMO, we considered target regions spanning the equator to 60° north over the Atlantic (0° to 80°W) and Pacific (120°E to 100°W) oceans (the areal mean over all SST gridboxes in each basin), and the full Northern Hemisphere (ocean + land). The CMIP5-All multimodel ensemble mean series (latitude weighted) for each of the target regions, along with the ensemble of individual simulations, were compared with the actual historical observations over the interval 1854–2012 C.E. (Fig. 1 and fig. S1) (*27*). We used Goddard Institute for Space Studies (GISS) Surface Temperature (GISTEMP) (*31*) for the observational NH mean (ocean + land) series, owing to recent evidence (*32*) that other products may underestimate recent warming by undersampling the Arctic. For the regional observational SST estimates, we used the mean of the Hadley Centre Global Sea Ice and Sea Surface Temperature (HadISST) (*33*), National Oceanic and Atmospheric Administration (NOAA) Extended Reconstructed Sea Surface Temperature (ERSST) (*34*, *35*), and Kaplan (*36*–*38*) products.

The results of the target-region regression analysis show for each of the three model ensembles that the estimated internal variability components derived from the various realizations are statistically independent, as they should be if the method is performing correctly, contrasting with what we find for the other previously used methods (Fig. 2, figs. S2 to S4, and table S2) (*27*). We next applied the methods in a semi-empirical setting in order to estimate the actual historical AMO, PMO, and NMO series. Under the assumption that the observational temperature series are the sum of a forced component and the real-word realization of internal variability, we estimate the true historical internal variability component as the residual series after the forced components are removed.

Our approach gives similar results whether CMIP5-All, CMIP5-GISS, CMIP5-AIE [or even individual models with a minimum of $n \geq 10$ realizations (fig. S6)] ensemble means are used (*39*). The root mean square amplitude of the AMO and PMO are similar for all three ensembles (0.10/0.11/0.09°C for AMO and 0.09/0.09/0.11°C for PMO, for CMIP5-All/CMIP5-GISS/CMIP5-AIE, respectively). Unlike with the linear detrending approach, the PMO and AMO are not found to be significantly correlated. An analysis of the full multimodel ensemble reveals any putative correlation between the AMO and PMO [and arguments of a "stadium wave" climate signal (*40*)] to be an artifact of the linear detrending approach (fig. S7) (*27*). Shown also (Fig. 3) are the results of a simple bivariate regression demonstrating that the NMO can be very closely approximated [coefficient of determination (R^2) = 0.86/0.88/0.91 for CMIP5-All/CMIP5-GISS/CMIP5-AIE, respectively] by a weighted combination of the AMO and PMO series (*41*). The amplitude of the NMO (0.07°C using either CMIP5-All or CMIP5-GISS, and 0.08°C using CMIP5-AIE) is consistent with results from long model control runs (*3*).

Our analysis shows the NMO to be decreasing at the end of the series (Fig. 3 and figs. S5 and S6). Mann *et al.* (*42*) assessed the recent decrease in the NMO in terms of a negative-trending AMO contribution. However, we reach a somewhat different conclusion in the present study, finding that the recent decrease in the NMO is instead a result of a sharply decreasing PMO (with a relatively flat AMO contribution). That observation is consistent with recent findings that the anomalous slowing of warming over the past decade

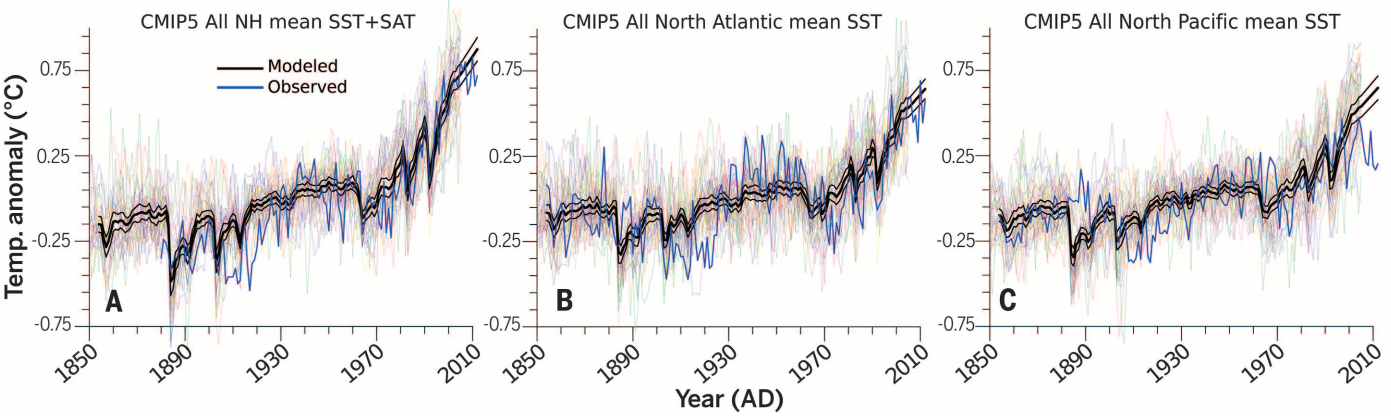

Fig. 1. CMIP5-All ensemble means shown with individual model means. (**A**) Northern Hemisphere SST+SAT. (**B**) North Atlantic SST. (**C**) North Pacific SST. Ensemble mean, black curves; individual model means, colored curves. Thin black line depicts the 95% confidence limits of the model mean determined via bootstrap resampling. Blue line depicts observed temperatures.

is tied to subsurface heat burial in the tropical Pacific and a tendency for persistent "La Niña"–like conditions (*43–46*). Our analysis attributes this trend to internal variability as a consequence of the failure of the CMIP5 models to identify a recent forced trend of this nature. However, there is paleoclimate evidence suggesting that a La Niña–like response might arise from positive radiative forcing (*47*), and the possibility remains that state-of-the-art climate models fail to capture such a dynamical response to anthropogenic radiative forcing.

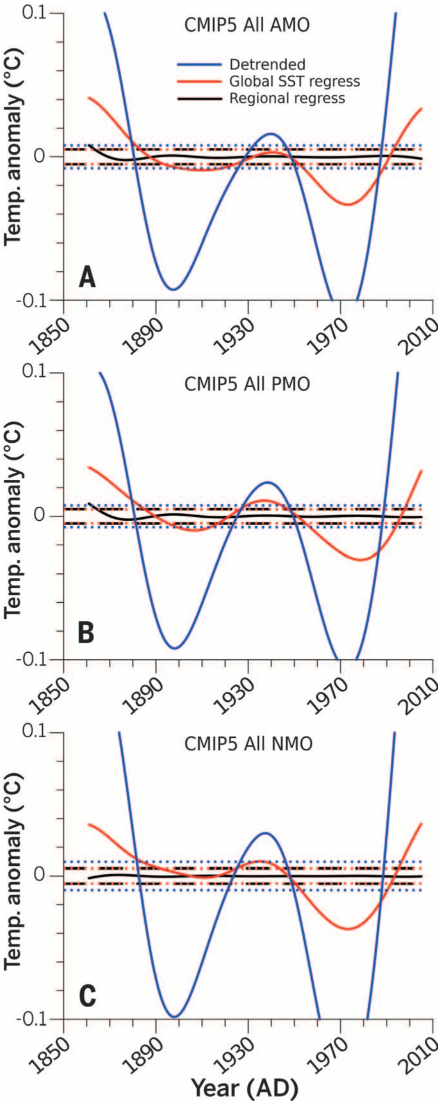

Fig. 2. CMIP5-All mean series and estimated 1-σ bounds for mean series under the assumption of statistical independence of internal variability among ensemble members. (**A**) AMO. (**B**) PMO. (**C**) NMO. Solid lines indicate mean of all realizations; dashed lines indicate estimated 1-σ bounds. Determined by using detrending (blue), global SST regression (red), and target region regression (black). Individual realizations of CMIP5-All internal variability as well as results for target region differencing are shown in the supplementary materials (fig. S2).

Some recent work (*18*, *19*, *21*, *22*, *25*) has attributed a potentially large proportion of observed regional and hemispheric temperature changes to multidecadal internal variability related to the so-called "AMO" and/or "PDO." Using the CMIP5 multimodel historical climate simulations, we have established that the methods used in these studies tend to inflate and distort the estimated internal variability owing to an incorrect partition of internal and forced variability. We have demonstrated that our target-region regression method correctly isolates the internal variability components.

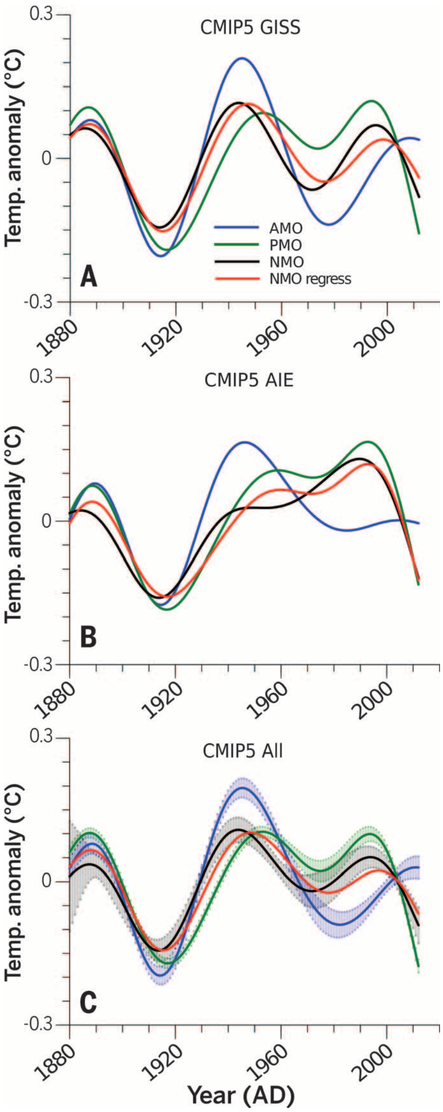

Fig. 3. Semi-empirical estimate of AMO, PMO, and NMO based on target region regression using historical climate model realizations. (**A**) CMIP5-GISS. (**B**) CMIP5-AIE. (**C**) CMIP-All. In (A) to (C), blue, AMO; green, PMO; and black, NMO. Bivariate regression-based approximation of NMO (red) strongly correlates (R^2 = 0.86/0.88/0.91 for CMIP5-All/CMIP5-GISS, CMIP5-AIE, respectively) with semi-empirical NMO estimate (black). 95% confidence limits of the AMO, PMO, and NMO CMIP5-All means were determined by using the ensemble of target region mean series resulting from bootstrap resampling (Fig. 1) and are shown as colored shading.

Applying our method to observational surface temperature data, we find that internal variability is likely to have had a substantial influence on multidecadal Northern Hemisphere temperature changes over the historical period, contributing up to 0.15°C peak warming/cooling. The AMO appears to have been influential in the early and middle 20th century, but the PMO has played a more dominant role in recent decades. This result is consistent across the three ensembles (GISS, AIE, and All) (Fig. 3). Our findings (the AIE experiments, especially) suggest that natural internal variability has had a modest influence on Atlantic SST over the past half century and that multidecadal climate variability attributed to Atlantic SST changes (such as variations in tropical storm frequency and strength and Sahel and Midwestern North American drought) (*48–51*) was largely driven by external forcing (as concluded in other recent work) (*52*). Our results also highlight the substantial uncertainties associated with the role of anthropogenic aerosol forcing in recent decades because the greatest discrepancies using the three different ensembles occur during that time period.

Our findings have strong implications for the attribution of recent climate changes. We find that internal multidecadal variability in Northern Hemisphere temperatures (the NMO), rather than having contributed to recent warming, likely offset anthropogenic warming over the past decade. This natural cooling trend appears to reflect a combination of a relatively flat, modestly positive AMO and a sharply negative-trending PMO. Given the pattern of past historical variation, this trend will likely reverse with internal variability instead, adding to anthropogenic warming in the coming decades.

REFERENCES AND NOTES

1. R. A. Kerr, *Science* **288**, 1984–1985 (2000).
2. T. L. Delworth, M. E. Mann, *Clim. Dyn.* **16**, 661–676 (2000).
3. J. R. Knight, R. J. Allan, C. K. Folland, M. Vellinga, M. E. Mann, *Geophys. Res. Lett.* **32**, L20708 (2005).
4. M. E. Mann, J. Park, *J. Geophys. Res.* **99** (D12), 25819 (1994).
5. N. J. Mantua, S. R. Hare, Y. Zhang, J. M. Wallace, R. C. Francis, *Bull. Am. Meteorol. Soc.* **78**, 1069–1079 (1997).
6. N. J. Mantua, S. R. Hare, *J. Oceanogr.* **58**, 35–44 (2002).
7. M. E. Mann, J. Park, *J. Clim.* **9**, 2137–2162 (1996).
8. M. E. Mann, J. Park, *Adv. Geophys.* **41**, 1–131 (1999).
9. S. Minobe, *Geophys. Res. Lett.* **24**, 683–686 (1997).
10. M. A. Alexander *et al.*, *J. Clim.* **15**, 2205–2231 (2002).
11. D. J. Vimont, *J. Clim.* **18**, 2080–2092 (2005).
12. W. Chen, B. Dong, R. Lu, *J. Geophys. Res.* **115** (D17), D17109 (2010).
13. B. Dong, R. T. Sutton, A. A. Scaife, *Geophys. Res. Lett.* **33**, L08705 (2006).
14. B. Guan, S. Nigam, *J. Clim.* **22**, 4228–4240 (2009).
15. G. J. van Oldenborgh, L. A. te Raa, H. A. Dijkstra, S. Y. Philip, *Ocean Sci.* **5**, 293–301 (2009).
16. C. Marini, C. Frankignoul, *Clim. Dyn.* **43**, 607–625 (2013).
17. S. B. Goldenberg, C. W. Landsea, A. M. Mestas-Nunez, W. M. Gray, *Science* **293**, 474–479 (2001).
18. M. G. Wyatt, S. Kravtsov, A. A. Tsonis, *Clim. Dyn.* **38**, 929–949 (2011).
19. M. G. Wyatt, J. A. Curry, *Clim. Dyn.* **42**, 2763–2782 (2013).

20. R. Zhang, T. L. Delworth, *Geophys. Res. Lett.* **34**, n/a (2007).
21. P. Chylek, J. D. Klett, G. Lesins, M. K. Dubey, N. Hengartner, *Geophys. Res. Lett.* **41**, 1689–1697 (2014).
22. M. Ting, Y. Kushnir, R. Seager, C. Li, *J. Clim.* **22**, 1469–1481 (2009).
23. K. E. Trenberth, D. J. Shea, *Geophys. Res. Lett.* **33**, L12704 (2006).
24. J. R. Knight, *J. Clim.* **22**, 1610–1625 (2009).
25. L. Terray, *Geophys. Res. Lett.* **39**, L19712 (2012).
26. K. E. Taylor, R. J. Stouffer, G. A. Meehl, *Bull. Am. Meteorol. Soc.* **93**, 485–498 (2012).
27. Materials and methods are available as supplementary materials on *Science* Online.
28. R. L. Miller *et al.*, *J. Adv. Model. Earth Syst.* **6**, 441–477 (2014).
29. M. Collins *et al.*, *Long-Term Climate Change: Projections, Commitments and Irreversibility*, T. F. Stocker *et al.*, Eds. (Cambridge Univ. Press, Cambridge, 2013), pp. 1029–1136.
30. G. A. Schmidt, D. T. Shindell, K. Tsigaridis, *Nat. Geosci.* **7**, 158–160 (2014).
31. J. Hansen, R. Ruedy, M. Sato, K. Lo, *Rev. Geophys.* **48**, RG4004 (2010).
32. K. Cowtan, R. G. Way, *Q. J. R. Meteorol. Soc.* **140**, 1935–1944 (2014).
33. N. A. Rayner, *J. Geophys. Res.* **108** (D14), 4407 (2003).
34. T. M. Smith, R. W. Reynolds, T. C. Peterson, J. Lawrimore, *J. Clim.* **21**, 2283–2296 (2008).
35. Y. Xue, T. M. Smith, R. W. Reynolds, *J. Clim.* **16**, 1601–1612 (2003).
36. A. Kaplan *et al.*, *J. Geophys. Res.* **103** (C9), 18,567–18,589 (1998).
37. D. E. Parker, P. D. Jones, C. K. Folland, A. Bevan, *J. Geophys. Res.* **99** (D7), 14373 (1994).
38. R. W. Reynolds, T. M. Smith, *J. Clim.* **7**, 929–948 (1994).
39. The regression analyses applied to the full CMIP5 multimodel mean yields a scaling factor ("beta") for Northern Hemisphere temperature changes that slightly exceeds unity (beta = 1.053 ± 0.0169), implying a real-world forced response that is slightly greater than that estimated by the CMIP5 multimodel mean. In contrast, North Atlantic mean temperatures yields a scaling factor slightly below unity (beta = 0.916 ± 0.0155), and North Pacific mean temperatures yield a scaling factor substantially below unity (beta = 0.629 ± 0.0182), suggesting that the CMIP5 multimodel mean substantially overestimates the amplitude of forced temperature changes over the North Pacific. Further details, including results for the two subensembles (CMIP5-A1E and CMIP5-GISS), are available in the supplementary materials (table S3).
40. S. Kravtsov, M. G. Wyatt, J. A. Curry, A. A. Tsonis, *Geophys. Res. Lett.* **41**, 6881–6888 (2014).
41. NMO = 0.35 AMO + 0.43 PMO for CMIP5-All; NMO = 0.42 AMO + 0.36 PMO for CMIP5-GISS; NMO = −0.06 AMO + 0.85 PMO for CMIP5-AIE; AMO and PMO regression coefficients are significant at the $P \ll 0.05$ level based on a one-sided test.
42. M. E. Mann, B. A. Steinman, S. K. Miller, *Geophys. Res. Lett.* **41**, 3211–3219 (2014).
43. K. E. Trenberth, J. T. Fasullo, *Earth's Future* **1**, 19–32 (2013).
44. M. H. England *et al.*, *Nature Clim. Change* **4**, 222–227 (2014).
45. Y. Kosaka, S.-P. Xie, *Nature* **501**, 403–407 (2013).
46. S. McGregor *et al.*, *Nature Clim. Change* **4**, 888–892 (2014).
47. M. E. Mann *et al.*, *Science* **326**, 1256–1260 (2009).
48. M. E. Mann, K. A. Emanuel, *Eos Trans. AGU* **87**, 233 (2006).
49. E. R. Martin, C. Thorncroft, *Geophys. Res. Lett.* **41**, 2169–2175 (2014).
50. J. R. Knight, C. K. Folland, A. A. Scaife, *Geophys. Res. Lett.* **33**, L17706 (2006).
51. Y. Kushnir, R. Seager, M. Ting, N. Naik, J. Nakamura, *J. Clim.* **23**, 5610–5628 (2010).
52. B. B. B. Booth, N. J. Dunstone, P. R. Halloran, T. Andrews, N. Bellouin, *Nature* **484**, 228–232 (2012).

ACKNOWLEDGMENTS

All raw data, Matlab code, and results from our analysis are available at the supplementary website: www.meteo.psu.edu/holocene/public_html/supplements/Science2015. We acknowledge the World Climate Research Programme's Working Group on Coupled Modeling, which is responsible for CMIP, and we thank the climate modeling groups for producing and making available their model output. We thank K. Emanuel and G. Schmidt for helpful comments on earlier versions of the manuscript. B.A.S. acknowledges support by the U.S. National Science Foundation Atmospheric and Geospace Sciences–Postdoctoral Research Fellowships (AGS-PRF) (AGS-1137750). Kaplan SST V2 data were provided by the NOAA/Office of Oceanic and Atmospheric Research/Earth System Research Laboratory Physical Sciences Division, Boulder, Colorado, USA: www.esrl.noaa.gov/psd. HadISST data were provided by the Met Office Hadley Centre: www.metoffice.gov.uk/hadobs. ERSST data were provided by NOAA: www.ncdc.noaa.gov/data-access/marineocean-data/extended-reconstructed-sea-surface-temperature-ersst-v3b.

SUPPLEMENTARY MATERIALS

www.sciencemag.org/content/347/6225/988/suppl/DC1
Materials and Methods
Supplementary Text
Figs. S1 to S7
Tables S1 to S3
References (*53*–*58*)

24 June 2014; accepted 26 January 2015
10.1126/science.1257856

PEST CONTROL

Full crop protection from an insect pest by expression of long double-stranded RNAs in plastids

**Jiang Zhang,[1] Sher Afzal Khan,[2] Claudia Hasse,[1] Stephanie Ruf,[1]
David G. Heckel,[2] Ralph Bock[1]***

Double-stranded RNAs (dsRNAs) targeted against essential genes can trigger a lethal RNA interference (RNAi) response in insect pests. The application of this concept in plant protection is hampered by the presence of an endogenous plant RNAi pathway that processes dsRNAs into short interfering RNAs. We found that long dsRNAs can be stably produced in chloroplasts, a cellular compartment that appears to lack an RNAi machinery. When expressed from the chloroplast genome, dsRNAs accumulated to as much as 0.4% of the total cellular RNA. Transplastomic potato plants producing dsRNAs targeted against the β-actin gene of the Colorado potato beetle, a notorious agricultural pest, were protected from herbivory and were lethal to its larvae. Thus, chloroplast expression of long dsRNAs can provide crop protection without chemical pesticides.

Double-stranded RNA (dsRNA) fed to insects can be taken up by midgut cells and processed into small interfering RNAs (siRNAs) by the insect's Dicer endoribonuclease (*1*–*3*). If the sequence of the fed dsRNA matches that of an insect gene, gene silencing by RNA interference (RNAi) disrupts expression of the insect's gene (*3*, *4*). By targeting essential insect genes, dsRNAs can be developed into highly species-specific insecticides (*4*). However, although expression of dsRNAs targeted against insect genes in transgenic plants (*1*, *2*, *5*–*8*) has impaired growth and development, complete protection of the plants and efficient killing of the insects have not been achieved. dsRNAs at least 60 base pairs (bp) in length are required for efficient uptake and biological activity in the target insect (*3*), but the plant's own system for producing small RNAs (*9*) prevents the accumulation of high amounts of long dsRNA. The major processing products of dsRNA cleavage by Dicer are 21-bp siRNAs, but these had little (*10*) or no effect when fed to insects (*3*). Thus, rapid turnover of dsRNAs in the plant limits the efficacy of transgenic RNAi-based anti-insect strategies.

The plastids (chloroplasts) of plant cells are derived from formerly free-living cyanobacteria, a group of prokaryotes that lack an RNAi pathway. We reasoned that chloroplasts might be capable of stably accumulating long dsRNAs, in which case dsRNA expression from the plastid genome could provide better protection against insect pests than dsRNA expression from the nuclear genome. To test the feasibility of stable dsRNA expression in plastids, we transformed the tobacco (*Nicotiana tabacum*) plastid genome with three different types of dsRNA constructs (Fig. 1A and fig. S1). In ptDP constructs, the dsRNA is generated by transcription from two convergent (dual) promoters. In ptSL constructs, the dsRNA is also produced from two convergent promoters, but each strand is additionally flanked by sequences forming stem-loop–type secondary structures, which increase RNA stability in plastids (*11*). In ptHP constructs, hairpin-type dsRNA (hpRNA) is produced by transcription of two transgene copies arranged as an inverted repeat (Fig. 1A). We targeted the Colorado potato beetle (*Leptinotarsa decemlineata*; CPB), a notorious insect pest of potato and other solanaceous crops (e.g., tomato and eggplant). Both larvae and adults feed on foliage, skeletonize the leaves, and, if left uncontrolled, completely destroy the crop. In many areas of the world, the beetle has no natural enemies, and chemical pesticides are the main method of CPB control. However, since the middle of the 20th century, CPB has developed resistance to all major insecticide classes (and therefore has been branded an "international superpest") (*12*).

---

[1] Max-Planck-Institut für Molekulare Pflanzenphysiologie, D-14476 Potsdam-Golm, Germany. [2] Max-Planck-Institut für Chemische Ökologie, D-07745 Jena, Germany.
***Corresponding author. E-mail: rbock@mpimp-golm.mpg.de**

Atlantic and Pacific multidecadal oscillations and Northern Hemisphere temperatures

Byron A. Steinman *et al.*

Science **347**, 988 (2015);
DOI: 10.1126/science.1257856

This copy is for your personal, non-commercial use only.

If you wish to distribute this article to others, you can order high-quality copies for your colleagues, clients, or customers by clicking here.

Permission to republish or repurpose articles or portions of articles can be obtained by following the guidelines here.

The following resources related to this article are available online at www.sciencemag.org (this information is current as of February 26, 2015):

Updated information and services, including high-resolution figures, can be found in the online version of this article at:
http://www.sciencemag.org/content/347/6225/988.full.html

Supporting Online Material can be found at:
http://www.sciencemag.org/content/suppl/2015/02/25/347.6225.988.DC1.html

A list of selected additional articles on the Science Web sites **related to this article** can be found at:
http://www.sciencemag.org/content/347/6225/988.full.html#related

This article **cites 54 articles**, 5 of which can be accessed free:
http://www.sciencemag.org/content/347/6225/988.full.html#ref-list-1

This article has been **cited by** 1 articles hosted by HighWire Press; see:
http://www.sciencemag.org/content/347/6225/988.full.html#related-urls

This article appears in the following **subject collections:**
Geochemistry, Geophysics
http://www.sciencemag.org/cgi/collection/geochem_phys

Downloaded from www.sciencemag.org on February 26, 2015

Science (print ISSN 0036-8075; online ISSN 1095-9203) is published weekly, except the last week in December, by the American Association for the Advancement of Science, 1200 New York Avenue NW, Washington, DC 20005. Copyright 2015 by the American Association for the Advancement of Science; all rights reserved. The title *Science* is a registered trademark of AAAS.